KEK Preprint 2018-4
May 2018
H

Versatile $e^+e^-/\gamma\gamma/ep$ facilities at a Future Circular Collider

R. BELUSEVIC

High Energy Accelerator Research Organization (KEK)
1-1 *Oho, Tsukuba, Ibaraki* 305-0801, *Japan*
belusev@post.kek.jp

Contents

Abstract : This note describes two versatile accelerator complexes that could be built at a Future Circular Collider (FCC) in order to produce e^+e^-, $\gamma\gamma$ and ep collisions. The first facility is an SLC-type machine comprising a superconducting L-band linear accelerator (linac) and two arcs of bending magnets inside the FCC tunnel. Accelerated by the linac, electron and positron beams would traverse the arcs in opposite directions and collide at centre-of-mass energies considerably exceeding those attainable at circular e^+e^- colliders. The proposed SLC-type facility would have the same luminosity as a conventional two-linac e^+e^- collider. The L-band linac may form a part of the injector chain for a 100-TeV proton collider inside the FCC tunnel (FCC-pp), and could deliver electron or positron beams for an ep collider (FCC-ep). The second facility is an ILC-based e^+e^- collider placed tangentially to the circular FCC tunnel. If the collider is positioned asymmetrically with respect to the FCC tunnel, electron (or positron) bunches could be accelerated by both linacs before they are brought into collision with the 50-TeV beams from the FCC-pp proton storage ring. The two linacs may also form a part of the injector chain for FCC-pp. Each facility could be converted into a $\gamma\gamma$ collider or a source of multi-MW beams for fixed-target experiments.

1 Introduction

The *Standard Model* (SM) of particle physics is supported by two theoretical 'pillars': the *gauge principle* and the *Higgs mechanism* for particle mass generation. Whereas the gauge principle has been firmly established through precision electroweak measurements, the Higgs mechanism is yet to be fully tested.

The SM predicts the existence of a neutral spin-0 particle with unique properties, the *Higgs boson*, but it does not predict its mass. The Higgs-boson mass, $m_{\rm H}$, affects the values of electroweak observables through radiative corrections. The best constraint on $m_{\rm H}$ is obtained by making a global fit to the electroweak data. Such a fit suggests that the most likely value of $m_{\rm H}$ is just above the limit of 114.4 GeV set by direct searches at LEP [1]. A particle consistent with the SM Higgs boson of mass $m_{\rm H} \approx 125$ GeV was discovered in 2012 at LHC [2, 3].

This shows that high-precision electroweak measurements provide a natural complement to direct studies of the Higgs sector. All the measurements made at LEP and SLC could be repeated at the facilities described in this note, but at much higher luminosities and by using 90% polarized electron beams [4].

The rich set of final states in e^+e^- and $\gamma\gamma$ collisions would play an essential role in measuring the mass, spin, parity, two-photon width and trilinear self-coupling of the SM Higgs boson, as well as its couplings to fermions and gauge bosons. Such measurements require centre-of-mass (c.m.) energies considerably exceeding those attainable at circular e^+e^- colliders. For instance, one has to measure separately the couplings HWW, HHH and Htt at $\sqrt{s_{ee}} \gtrsim 500$ GeV in order to determine the corresponding SM loop contributions to the effective HZZ coupling (see , e.g, [5]).

The maximum luminosity at a circular e^+e^- collider (such as the proposed FCC-ee facility [6] inside the FCC tunnel), is severely constrained by beamstrahlung effects at high energies; also, it is very difficult to achieve a high degree of beam polarization [7]. This is not the case at an SLC-type facility or a conventional two-linac e^+e^- collider, where luminosity is proportional to beam energy and the electron beam polarization can reach about 90%. The availability of polarized beams is essential for some important precision measurements in e^+e^- and $\gamma\gamma$ collisions [8].

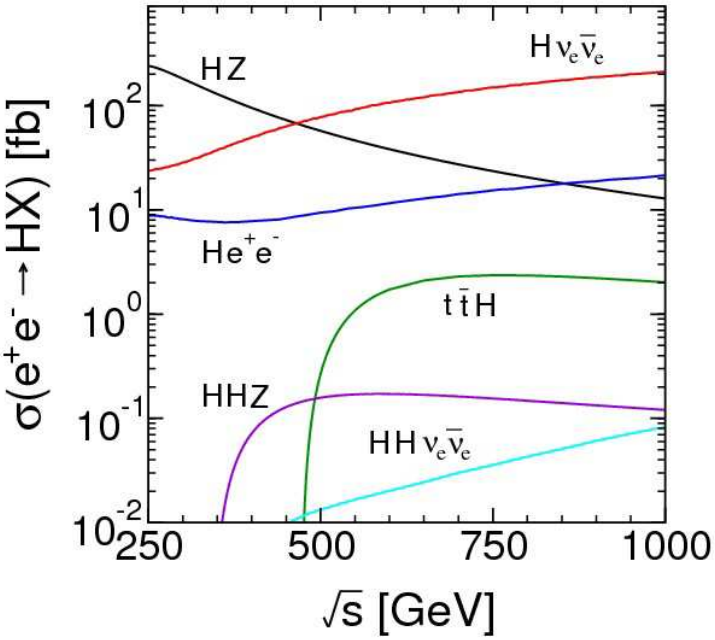

Figure 1: Centre-of-mass energy dependence of various cross-sections for single and double SM Higgs-boson production in e^+e^- annihilations [9].

If high-energy electron or positron bunches, accelerated by a superconducting L-band linac, are brought into collision with the proton beams from a 100-TeV hadron collider inside the FCC tunnel (FCC-pp), one would obtain an important source of deep-inelastic *ep* interactions. Such interactions would yield valuable information on the quark-gluon content of the proton, which is crucial for precision measurements at FCC-pp [10]. Note that FCC-ee and FCC-pp could be converted into an *ep* collider only if the FCC tunnel is wide enough, or if two concentric tunnels are built to accommodate both machines concurrently.

An SLC-type facility or a conventional two-linac collider could be constructed in several stages, each with distinct physics objectives that require particular c.m. energies (see Fig. 1):

- $e^+e^- \to$ Z, WW; $\quad \gamma\gamma \to$ H $\qquad\qquad \sqrt{s_{ee}} \sim 90$ to 180 GeV
- $e^+e^- \to$ HZ $\qquad\qquad \sqrt{s_{ee}} \sim 250$ GeV
- $e^+e^- \to t\bar{t}$; $\quad \gamma\gamma \to$ HH $\qquad\qquad \sqrt{s_{ee}} \sim 350$ GeV
- $e^+e^- \to$ HHZ, H$t\bar{t}$, H$\nu\bar{\nu}$ $\qquad\qquad \sqrt{s_{ee}} \gtrsim 500$ GeV

For some processes within and beyond the SM, the required c.m. energy is considerably lower in $\gamma\gamma$ collisions than in e^+e^- or proton-proton interactions. For example, the heavy neutral MSSM Higgs bosons can be created in e^+e^- annihilations only by associated production ($e^+e^- \to H^0A^0$), whereas in $\gamma\gamma$ collisions they are produced as single resonances ($\gamma\gamma \to H^0$, A^0) with masses up to 80% of the initial e^-e^- collider energy.

It is straightforward to convert an SLC-type facility or a conventional two-linac collider into a high-luminosity $\gamma\gamma$ collider with highly polarized beams. The CP properties of any neutral Higgs boson produced at a photon collider can be directly determined by controlling the polarizations of Compton-scattered photons (see [11] and references therein).

2 An SLC-type facility at FCC for creating $e^+e^-/\gamma\gamma/ep$ collisions

A schematic layout of an SLC-type $e^+e^-/\gamma\gamma$ facility at a Future Circular Collider (FCC) is shown in Fig. 2. Damped and bunch-compressed electron and positron beams, accelerated by a single superconducting L-band linac, traverse two arcs of bending magnets in opposite directions and collide at an interaction point surrounded by a detector. The beams are then disposed of, and this machine cycle is repeated at a rate of up to 10 Hz. In contrast to a conventional two-linac collider, an SLC-type machine would have a single bunch compression system.

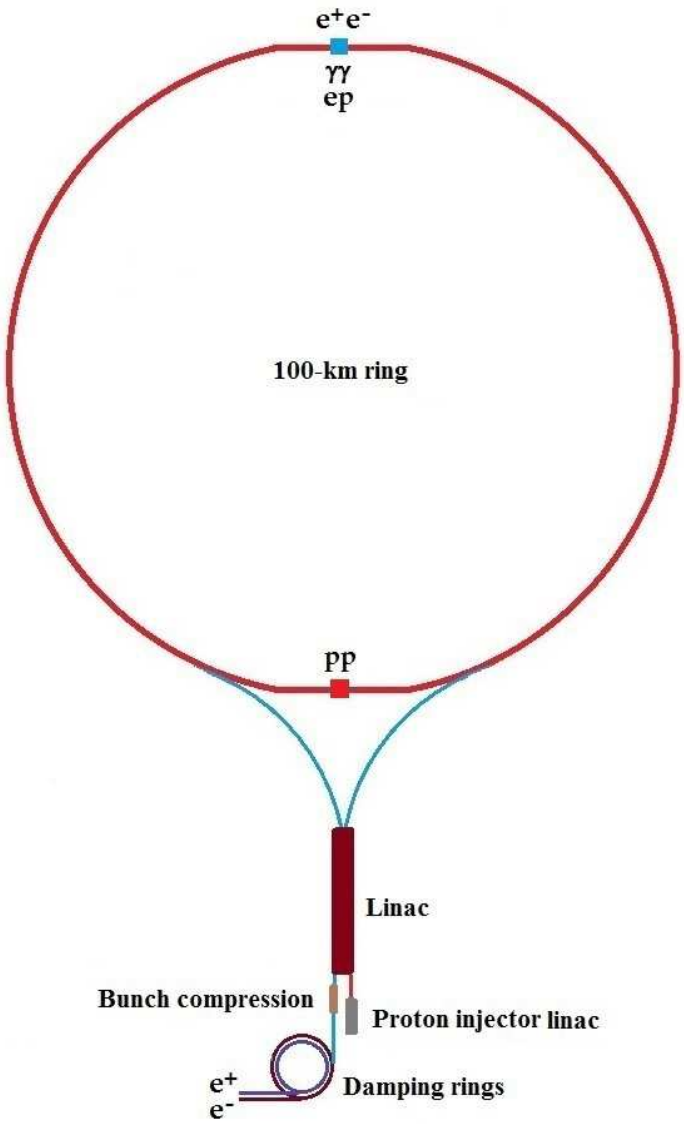

Figure 2: Schematic layout of an SLC-type facility at FCC. The superconducting L-band linac could be a part of the FCC-pp injector chain, and may also be used to produce multi-MW beams for fixed-target experiments. The entire accelerator complex would serve as a source of e^+e^-, $\gamma\gamma$, pp and ep interactions [11].

With a crossing angle at the interaction point (IP), separate beam lines may be used to bring the disrupted beams to their respective dumps, thereby enabling post-IP diagnostics. It is also envisaged that a 'bypass line' for low-energy beams would be employed to accumulate data at the Z resonance in the process $e^+e^- \to \mathrm{Z}$. The proposed facility could be constructed in several stages, each with distinct physics objectives that require particular c.m. energies (see the Introduction).

The linac at the proposed SLC-type facility would contain ILC-type superconducting L-band cavities placed within cryogenic vessels and fed by multi-beam klystrons. The current design for the *International Linear Collider* (ILC), based on the superconducting technology originally developed at DESY, uses L-band (1.3 GHz) superconducting niobium rf cavities that have average accelerating gradients of 31.5 MeV/m (see [12] and references therein). Nine cavities, each 1 m long, are mounted together in a string and assembled into a common low-temperature cryostat or *cryomodule*. Liquid helium is used to cool cavities to -271° C.

An ILC-type main linac is composed of rf units, each of which is formed by three contiguous cryomodules containing 26 nine-cell cavities. Every unit has an rf source, which includes a pulse modulator, a 10 MW multi-beam klystron, and a waveguide system that distributes the power to the cavities. An ILC-type design has the following characteristics:

- Transverse wakefield effects are drastically reduced due to the large size of L-band cavities, which means that cavity alignment tolerances can be relaxed. This is particularly relevant for an SLC-type facility, where both e^+ and e^- bunches are alternately accelerated;
- Superconducting SLC-type rf cavities can be loaded using a long rf pulse (~ 1.5 ms) from a source with low peak rf power;
- 'Wall-plug to beam' power transfer efficiency is, for example, about twice that of X-band cavities, which makes an IC-type linac much cheaper to operate;
- The long rf pulse allows a long 'bunch train' (~ 1 ms), with many bunches (~ 3000) and a relatively large bunch spacing ($\gtrsim 300$ ns). A trajectory correction (feedback) system within the train can therefore be used to bring the beams into collision.

At an SLC-type facility, e^+ and e^- bunches are alternately accelerated inside the linac. In order to focus electron and positron beams in the two transverse planes, quadrupole magnets with alternating polarities have to be placed along the linac. The x-plane for electrons is then like the y-plane for positrons, and vice versa. At the Stanford Linear Collider, emittance growth in the linac was reduced using the beam diagnostics obtained by steering both beams together [13].

The spacing between electron bunches in a superconducting L-band accelerator can be made to match that between the proton bunches in the FCC-pp storage ring. Also, the length of an electron 'bunch train' corresponds roughly to the FCC ring circumference. An ILC-type linac is thus a suitable source of electron beams for an electron-proton collider. Accelerated by the linac, electron or positron beams would traverse one of the two arcs of bending magnets inside the FCC tunnel and collide with the 50-TeV beams from the FCC-pp proton storage ring (see Fig. 2).

The *energy loss* per turn due to *synchrotron radiation* (SR) in an electron storage ring is given by the expression

$$\Delta \mathrm{E} \,=\, C_\gamma \frac{\mathrm{E}_0^4}{\rho} \qquad \Rightarrow \qquad \mathrm{E}(s) \,=\, \mathrm{E}_0 \Big(1 \,+\, \frac{A}{\rho^2} s \Big)^{-1/3} \tag{1}$$

where $C_\gamma = 88.46 \times 10^{-6}$ m/GeV^3, E [GeV] is the beam energy, ρ [m] is the *effective bending radius*, s [m] is the beam path length, and $A \equiv 3 C_\gamma \mathrm{E}_0^3 / 2\pi$. For $\mathrm{E}_0 = 250$ GeV and $\rho = 12$ km, the total energy loss in each bending arc of the proposed SLC-type facility is $\Delta \mathrm{E} = 14.4$ GeV.

The *energy spread* in a circulating electron beam due to SR is given by

$$\frac{\sigma_\mathrm{E}}{\mathrm{E}} \,\approx\, \gamma \sqrt{\frac{C_q}{2\rho}} \tag{2}$$

where γ is the Lorentz factor of the beam, $C_q \approx 3.84 \times 10^{-13}$ m, and ρ [m] is the bending radius. For $\mathrm{E} = 250$ GeV and $\rho = 12$ km, Eq. (2) yields $\sigma_\mathrm{E}/\mathrm{E} \approx 6 \times 10^{-4}$. A plot of $\sigma_\mathrm{E}/\mathrm{E}$ as a function of beam energy is shown in Fig. 6 of [11]. For electron beams with $\mathrm{E} \lesssim 450$ GeV traversing the bending arcs of the proposed SLC-type facility, the increase in the *horizontal beam emittance* would not exceed $2\,\mu m$, the value of this parameter at the KEK–ATF damping ring (see Fig. 7 in [11]).

An important feature of the proposed facility is the possibility of using backscattered laser beams to produce high-energy $\gamma\gamma$ collisions [14]. In order to attain maximum luminosity at a $\gamma\gamma$ collider, every electron bunch in the accelerator should collide with a laser pulse of sufficient intensity for 63% of the electrons to undergo a Compton scattering. This requires a laser system with high average power, capable of producing pulses that would match the temporal spacing of electron bunches. These requirements could be satisfied by an optical *free electron laser* [15].

Assuming that the mean number of Compton interactions of an electron in a laser pulse (the Compton conversion probability) is 1, the *conversion coefficient*

$$k \equiv N_\gamma/N_e \approx 1 - \mathrm{e}^{-1} = 0.63 \tag{3}$$

where N_e is the number of electrons in a 'bunch' and N_γ is the number of scattered photons. The luminosity of a gamma-gamma collider is then

$$\mathcal{L}_{\gamma\gamma} \;=\; (N_\gamma/N_e)^2\,\mathcal{L}_{ee} \;\approx\; (0.63)^2\,\mathcal{L}_{ee} \tag{4}$$

where $\mathcal{L}_{ee}$ is the *geometric luminosity* at a conventional two-linac collider:

$$\mathcal{L}_{ee} \;\propto\; \frac{\gamma N_e^{\,2} N_b f_{\rm rep}}{\sqrt{(\varepsilon_x^n\beta_x^*)(\varepsilon_y^n\beta_y^*)}} \;\equiv\; \frac{\mathcal{P}_b}{\sqrt{s_{ee}}}\,\frac{\gamma N_e}{\sqrt{(\varepsilon_x^n\beta_x^*)(\varepsilon_y^n\beta_y^*)}} \tag{5}$$

In this expression, β_x^* and β_y^* are the horizontal and vertical *beta functions* at IP, respectively, ε_x^n and ε_y^n are the normalized transverse *beam emittances*, N_b is the number of bunches per rf pulse, $f_{\rm rep}$ is the pulse *repetition rate*, $\sqrt{s_{ee}}$ is the c.m. energy, $\mathcal{P}_b = N_e N_b f_{\rm rep}\sqrt{s_{ee}}$ is the *beam power*, and $\gamma \equiv \mathrm{E}/m_e c^2$ is the *Lorentz factor* of the electron beam with energy E (see Table 1).

There are $N_b/2$ electron or positron bunches in each arc of an SLC-type facility. If its repetition rate is twice that of a conventional two-linac collider, so that roughly the same wall-plug power is used, the two machines would have the same luminosity (see Eq. (5)).

3 An ILC-based $e^+e^-/\gamma\gamma/ep$ facility at FCC

An ILC-based $e^+e^-/\gamma\gamma/ep$ facility at a Future Circular Collider (FCC) is shown in Fig. 3. A superconducting two-linac e^+e^- collider is placed tangentially to the circular FCC tunnel. Using an optical free-electron laser, the linacs could be converted into a high-luminosity $\gamma\gamma$ collider.

The maximum c.m. energy of the SLC-type facility described in the previous section is limited by the radius of the bending arcs, which is not the case with a conventional two-linac e^+e^- collider. Note also that the asymmetric accelerator configuration in Fig. 3 allows one to double the energy of electron, positron or proton beams before their extraction (see Section 4).

The baseline parameters for the proposed ILC collider, shown in Table 1, reflect the need to balance the constraints imposed by the various accelerator sub-systems, as explained in [16]. The rf power is provided by 10 MW multi-beam klystrons, each driven by a 120 kV pulse modulator. The estimated AC power is 122 MW at $\sqrt{s_{ee}} = 250$ GeV and 163 MW at $\sqrt{s_{ee}} = 500$ GeV.

In order to maximize luminosity at low c.m. energies, the beam power could be increased by increasing the pulse repetition rate $f_{\rm rep}$, while reducing the accelerating gradient of the main linacs. At $\sqrt{s_{ee}} = 250$ GeV, the power consumption of the main linacs is reduced by over a factor of two when they are running at approximately half their nominal gradient. This enables one to run the accelerator at its maximum repetition rate $f_{\rm rep} = 10$ Hz, thus doubling the luminosity.

As mentioned in the Introduction, the maximum luminosity at a circular e^+e^- collider is severely constrained by beamstrahlung effects at high energies; also, it is very difficult to achieve a high degree of beam polarization. This is not the case at an SLC-type facility or a conventional two-linac e^+e^- collider, where luminosity is proportional to beam energy and the electron beam polarization can reach about 90%.

Table 1: Baseline ILC parameters [16]

Centre-of-mass energy	$\sqrt{s_{ee}}$	GeV	250	500
Pulse repetition rate	$f_{\rm rep}$	Hz	5	5
Bunch population	N_e	$\times 10^{10}$	2	2
Number of bunches	$N_{b,e}$		1312	1312
Bunch interval	$\Delta t_{b,e}$	ns	554	554
RMS bunch length	$\sigma_{z,e}$	mm	0.3	0.3
Norm. horizontal emittance at IP	ε_x^n	μm	10	10
Norm. vertical emittance at IP	ε_y^n	nm	35	35
Horizontal beta function at IP	β_x^*	mm	13	11
Vertical beta function at IP	β_y^*	mm	0.41	0.48
RMS horizontal beam size at IP	σ_x^*	nm	729	474
RMS vertical beam size at IP	σ_y^*	nm	7.7	5.9
Vertical disruption parameter	D_e		24.5	24.6
Luminosity	$\mathcal{L}_{ee}$	$\times 10^{34}\ cm^{-2}\, s^{-1}$	0.75	1.8

The two superconducting L-band linac in Fig. 3 may also form a part of the FCC-pp injector chain. Since the collider is positioned asymmetrically with respect to the FCC tunnel, electron (or positron) bunches could be accelerated by both linacs before they are brought into collision with the 50-TeV beams from the FCC-pp proton storage ring, as mentioned above. The entire accelerator complex would serve as asource of e^+e^-, $\gamma\gamma$, *pp* and *ep* interactions.

4 Main parameters of a linac-ring *ep* collider at FCC

The idea to combine a 140-GeV electron linac and a 20-TeV proton storage ring in order to produce *ep* interactions at very high c.m. energies was put forward in 1979 as a possible option at the SSC proton collider [17]. In 1987 it was proposed to place a 2-TeV linear e^+e^- collider (VLEPP) tangentially to a 6-TeV proton-proton collider (UNK) at IHEP in Protvino [18], with the aim of obtaining both *ep* and γp collisions. Similar proposals for lepton-hadron and photon-hadron colliders at HERA, LHC and FCC have since been made (see [19] and references therein).

The SLC-type facility in Fig. 2 could be used to produce TeV-scale *ep* interactions. Accelerated by the superconducting L-band linac, electron or positron beams would traverse one of the two arcs of bending magnets inside the FCC tunnel and collide with the FCC-pp proton beams.

The facility shown in Fig. 3 is an ILC-based version of the original VLEPP⊗UNK design. Since the collider is positioned asymmetrically with respect to the FCC tunnel, electron (or positron) bunches could be accelerated by both linacs (which contain *standing wave cavities*) before they are brought into collision with the 50-TeV beams from the FCC-pp proton storage ring.

In Section 2 it was noted that an ILC-type linac is a suitable source of electron beams for an electron-proton collider, because: (1) the spacing between electron bunches can be made to match that between the proton bunches in the FCC-pp storage ring, and (2) the length of an electron 'bunch train' corresponds roughly to the FCC ring circumference.

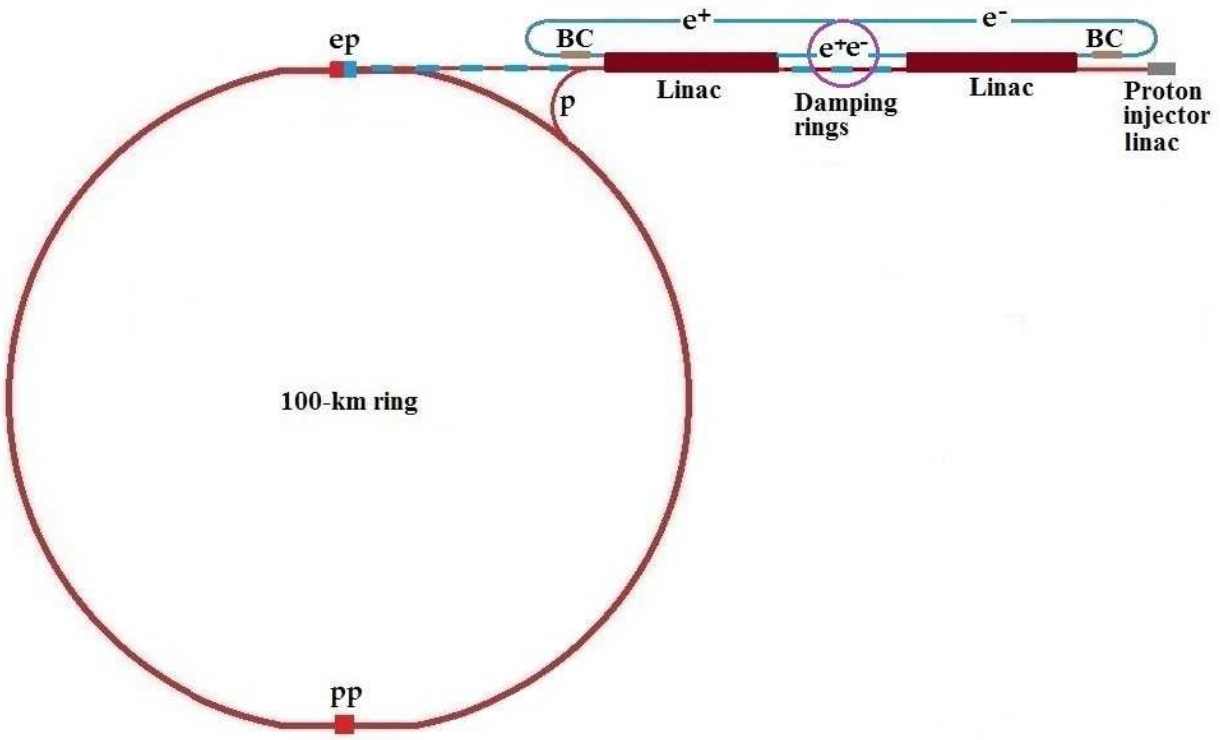

Figure 3: Schematic layout of an ILC-based facility at FCC (BC stands for *bunch compression*). Electron (or positron) bunches are accelerated by both linacs before their collision with the 50-TeV proton beam from the FCC-pp storage ring. The two superconducting L-band linacs may form the low-energy part of the FCC-pp injector chain.

In *head-on collisions* of ultra-relativistic electrons and protons, the centre-of-mass energy is $\sqrt{s_{ep}} = 2\sqrt{\mathrm{E}_e \mathrm{E}_p}$. The total electron beam current $I_e = \mathcal{P}_e/\mathrm{E}_e$ is limited by the maximum allowed beam power $\mathcal{P}_e$ for a given electron beam energy E_e. Assuming that round electron and proton beams of equal transverse sizes are colliding head-on at the interaction point (IP),[1] the luminosity of the collider is given by [20][21]

$$\mathcal{L}_{ep} = f_c \frac{N_e N_p}{4\pi\sigma_p^2}\,\mathcal{H} \equiv \frac{I_e}{4\pi \mathrm{e}}\frac{N_p}{\varepsilon_p^n}\frac{\gamma_p}{\beta_p^*}\,\mathcal{H} \tag{6}$$

In these expressions, N_e and N_p are the electron and proton bunch populations, respectively; f_c is the bunch collision frequency; $\mathcal{H}$ is a correction factor discussed below; and $\sigma_p = \sqrt{\varepsilon_p^n \beta_p^*/\gamma_p}$ is the proton beam size at IP, expressed in terms of the normalized proton beam emitance, ε_p^n, the proton beta function at IP, β_p^*, and the Lorentz factor of the proton beam, γ_p. Note that the luminosity is proportional to the electron beam power $\mathcal{P}_e = \mathrm{e}N_e f_c \mathrm{E}_e = I_e \mathrm{E}_e$ (e is the electron charge), the proton beam energy (γ_p), and the proton beam brightness N_p/ε_p^n.

In Eq. (6), $\mathcal{H}$ is a product of three correction factors with values typically close to unity:

$$\mathcal{H} \equiv H_{\mathrm{hourglass}} \cdot H_{\mathrm{pinch}} \cdot H_{\mathrm{filling}} \tag{7}$$

The factor H_{filling} takes into account the filling patterns of the electron and proton beams. If the number of proton bunches $N_{b,p} = 10600$ and the bunch interval $\Delta t_{b,p} = 25$ ns (see Table 2), the 'length' of the proton beam is 2.65×10^5 ns. This corresponds to 80 km, which means that only 80% of the FCC circumference is filled with proton bunches ($H_{\mathrm{filling}} = 0.8$). In this particular case 20% of the electron bunches would not collide with the proton beam.

[1]The two beams are chosen to have roughly equal transverse sizes in order to reduce adverse effects a much smaller electron beam could have on the proton beam lifetime. Electron bunches are discarded after each collision.

Table 2: Baseline FCC-pp parameters [22][23]. Numbers inside round brackets represent parameters for 5 ns bunch spacing.

Beam energy	E_p	TeV	50
Initial bunch population	N_p	$\times 10^{10}$	10 (2)
Number of bunches	$N_{b,p}$		10600 (53000)
Bunch interval	$\Delta t_{b,p}$	ns	25 (5)
RMS bunch length	$\sigma_{z,p}$	mm	80
Norm. transverse emittance	ε_p^n	μm	2.2 (0.44)
Beta function at IP	β_p^*	m	0.3
Beam size at IP	σ_p	μm	6.8 (3)
Beam-beam tune shift/IP	ΔQ_p		0.005
Luminosity/IP	$\mathcal{L}_{ep}$	$\times 10^{32}\ cm^{-2}\,s^{-1}$	2.3

The factor $H_{\rm hourglass}$ accounts for a loss of luminosity when the bunch length is comparable to or larger than β^*. The beta function $\beta(s) = \beta^* + s^2/\beta^*$ grows parabolically as a function of distance s from the interaction point, which causes the beam size to increase:

$$\sigma(s) = \sqrt{\beta(s)\cdot\varepsilon} \approx s\sqrt{\varepsilon/\beta^*} \tag{8}$$

As the beam size increases, the contribution to the luminosity from regions with large σ decreases (*hourglass effect*). For zero crossing angle and $\sigma_{z,p} \gg \sigma_{z,e}$,

$$H_{\rm hourglass}(x) = \sqrt{\pi}\, x\, {\rm e}^{x^2}\, {\rm erfc}(x) \tag{9}$$

with

$$x \equiv \frac{2\beta_e^*}{\sigma_{z,p}} \frac{\varepsilon_e/\varepsilon_p}{\sqrt{1+(\varepsilon_e/\varepsilon_p)^2}}, \qquad\qquad {\rm erfc}(x) = \frac{2}{\sqrt{\pi}} \int_x^\infty {\rm e}^{-t^2}\, {\rm d}t \tag{10}$$

where ε_e and ε_p denote *geometric emittances* [10][24] (the normalized emittance $\varepsilon^n = \gamma\varepsilon$ is invariant under acceleration); erfc(z) is the 'complementary error function' (defined as the area under the 'tails' of a Gaussian distribution).

The enhancement factor $H_{\rm pinch}$ in Eq. (7) is due to the attractive *beam-beam force*. Since the electron bunch charge is relatively small and the proton energy is high, the beam-beam force acting on electrons has a much greater strength than that acting on protons. Consequntly, the electron bunch is focused by the protons during a collision,. This leads to a reduction in the transverse electron beam size ('pinch effect') and hence to an increase in the luminosity. The effect can be simulated using the program *Guinea-Pig* (see [25] and references therein, as well as Table 3 below).

One can ignore the longitudinal structure of electron bunches because they are much shorter than proton bunches. In this case the *transverse disruption* of the electron beam during a collision is described by the parameter [26]

$$D_e = \frac{r_e}{\gamma_e} \frac{N_p \sigma_{z,p}}{\sigma_p^2} \tag{11}$$

where γ_e is the Lorentz factor of the electron beam, $r_e \approx 2.82 \times 10^{-15}$ m is the classical radius of the electron, and $\sigma_{z,p}$ is the proton bunch length (see Fig. 4). For $\beta_p^* = 10$ cm, the disruption parameter can be as large as $D_e \approx 20$ in an *ep* linac-ring collider.

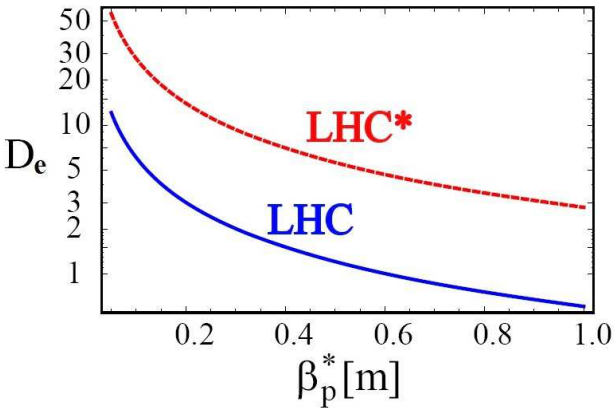

Figure 4: Electron beam disruption parameter D_e as a function of β_p^* [21]. The plot was made for an *ep* collider based on LHC and an ILC-type electron linac. LHC* denotes an upgraded proton beam scenario (see Table 1 in [21]).

As already mentioned, the luminosity of an *ep* collider is proportional to the proton *beam brightenss* $N_p/\varepsilon_p^{\mathrm{N}}$ (see Eq. (6)). Together with a given bunch length and energy spread, the beam brightness is a measure of the phase-space density. In the low-energy part of a proton injector, the quantity N_p/ε_p^n is limited by space-charge forces that induce a *transverse tune shift*[2]

$$\Delta Q_{sc} \propto \frac{N_p}{\varepsilon_p^n} \frac{1}{(v_p/c)^2 \gamma_p^2} \tag{12}$$

Here v_p is the proton velocity and c is the speed of light in vacuo [27][28]. In order to reduce the effect of space-charge forces at low energies, the facility in Fig. 3 features a single 3-GeV proton injector linac.

At high energies, the beam brightness in a storage ring slowly diminishes due to Coulomb scattering of protons within a bunch (*intra-beam scattering*) [29]. In the presence of *dispersion* (see footnote 3), the intra-beam scattering also leads to an increase in emittance. This sets the ultimate limit on the phase-space density in a proton storage ring. The growth of a beam of charged particles due to intra-beam scattering is characterized by the horizontal *growth rate* [30]

$$\tau_x^{-1} \propto \frac{N_p}{\varepsilon_x^n \varepsilon_y^n \varepsilon_l^n} \tag{13}$$

where $\varepsilon_{x,y}^n$ are the normalized beam emittances, $\varepsilon_l^n \equiv \beta\gamma\sigma_{z,p}\sigma_{\Delta p/p}$ and $\sigma_{\Delta p/p}$ is the r.m.s. relative momentum $\Delta p/p$. Note that the growth rate depends linearly on the normalized phase-space density.

The space-charge forces that limit the beam brightness are determined by the longitudinal charge density and thus by the proton bunch length $\sigma_{z,p}$. To attain maximum brightness, $\sigma_{z,p}$ should be as large as possible. On the other hand, there is a loss of luminosity when the bunch length is comparable to or larger than β^* (this *hourglass effect* was described earlier). Furthermore, the transverse disruption of the electron beam during an *ep* collision is proportional to $\sigma_{z,p}$, as shown in Eq. 11. While optimizing the bunch length within these constraints, the beam stability must be preserved (see below).

A particle in one colliding beam experiences a force due to the electromagnetic interactions with all the particles in the opposing beam. This force depends upon the displacement of the

[2]The 'tune' or Q value is defined as the number of betatron oscillations per revolution in a circular accelerator. The charge and current of a high-inensity beam in an accelerator create self-fields and image fields that alter the beam dynamics and influence the single-particle motion as well as coherent oscillations of the beam as a whole. The effect of space-charge forces is to change Q by an amount ΔQ_{sc} ('tune shift') [27].

particle from the equilibrium orbit of the opposing bunch. For small particle displacements, the beam-beam interaction is nearly linear, and its strength is characterized by a parameter known as the *beam-beam tune shift* [31]:

$$\Delta Q_p \equiv \frac{r_p}{4\pi}\frac{N_e}{\sigma_e^2}\frac{\beta_p^*}{\gamma_p} \approx \frac{r_p N_e}{4\pi\varepsilon_p^n} \tag{14}$$

Since electron bunches are discarded after each collision, only the tune shift of the proton beam, ΔQ_p, is considered here. In Eq. (14), $r_p \approx 1.53 \times 10^{-18}$ m is the classical radius of the proton, and $\sigma_p \approx \sigma_e$ was used. The tune shift is approximately given by

$$\Delta Q_p \approx 1.2 \times 10^{-3} \cdot \frac{N_e[10^{10}]}{\varepsilon_p^n[10^{-6}\,m]} \tag{15}$$

The parameter ΔQ_p must be limited to about 4×10^{-3} in order to stem the emittance growth due to random fluctuations of the electron bunch parameters [32]. This imposes an upper limit of $N_e \lesssim 3 \times 10^{10}$ if one assumes $\varepsilon_p^n \approx 10^{-6}$ m (see also Table 4 in [33]).

A small error Δk in the quadrupole gradient leads to a tune shift ΔQ_k. To a beam particle with momentum $p = p_0 + \Delta p$ it appears that all the quadrupoles in the ring have a quadrupole error proportional to $\Delta p/p_0$ [34]. The dimensionless quantity ξ defined by $\Delta Q_k \equiv \xi(\Delta p/p_0)$ is called the *chromaticity* of the beam optics. This quantity increases with the strength of the beam focusing. The main contribution to the chromaticity comes from the final focus quadrupoles, where the β-function is large [35]:

$$\xi \approx \beta_q k_q \ell_q \approx \frac{\ell^* + \ell_q/2}{\beta_y^*} \tag{16}$$

Here β_q, k_q and ℓ_q denote the beta function, field gradient and length of the final quadrupole, respectively; ℓ^* is the focal length and β_y^* the value of the vertical β-function at the interaction point. Thus, the chromaticity increases as β_y^* decreases.

Since ξ grows linearly with the distance between the final-focus quadrupole and the interaction point, it is desirable to make this distance as small as possible. For the interaction region at an electron-proton collider, a novel design technique called the *achromatic telescopic squeezing* (ATS) has been proposed "in order to find the optimal solution that would produce the highest luminosity while controlling the chromaticity, minimizing the synchrotron radiation power and maintaining the dynamic aperture required for [beam] stability" [36].

The issue of beam stability was addressed earlier concerning the optimization of the proton bunch length. Since the proton bunches inside the ILC-type linac shown in Figs 2 and 3 are much shorter than those inside the FCC storage ring, $\sigma_{z,p}$ has to be increased in order to attain the baseline FCC-pp value (see Table 2). In principle, the easiest way to increase the bunch length in a circular accelerator is to switch all RF systems off and let the bunches 'decay' due to *dispersion*.[3] A faster and more subtle procedure is described, e.g., in [37]. Bunch 'streching' could be carried out inside the FCC's high-energy booster.

The analytic expressions for beam-beam tune shift, electron beam disruption and beam growth rate given above do not accurately describe the *time-dependent beam dynamics* during collisions. To study the time-dependent effects caused by varying beam sizes, collision point simulations for linac-ring *ep* colliders have been performed using the ALOHEP software [38]. This numerical program optimizes a set of electron and proton beam parameters in order to maximize luminosity. Some of the results obtained by the program are presented in [39].

[3] A particle with a momentum difference $\Delta p/p$ has a transverse position $x(s) + D(s)\Delta p/p$, where $x(s)$ is the position a particle of nominal momentum would have and $D(s)$ is the *dispersion function*.

Table 3: Parameters of the proposed linac-ring *ep* collider.

Electron beam parameters			
Beam energy	E_e	GeV	500
Initial bunch population	N_e	$\times 10^{10}$	2
Number of bunches	$N_{b,e}$		3200
Bunch interval	$\Delta t_{b,e}$	ns	211.376
RF frequency	f_{RF}	MHz	1301
Pulse repetition rate	f_{rep}	Hz	5
Duty cycle	d	%	0.34
Beam power	$\mathcal{P}_e$	MW	25.5
Proton beam parameters			
Beam energy	E_p	TeV	50
Initial bunch population	N_p	$\times 10^{10}$	10
Number of bunches	$N_{b,p}$		5300
RMS bunch length	$\sigma_{z,p}$	mm	80
Bunch interval	$\Delta t_{b,p}$	ns	49.7355
RF frequency	f_{RF}	MHz	401.968
Collider parameters			
Beta function at IP	β_p^*	m	0.1
Norm. transverse emittance	ε_p^n	μm	1
Beam-beam tune shift	ΔQ_p		0.0024
Electron beam disruption	D_e		11.3
Hourglass factor	$H_{\mathrm{hourglass}}$		0.81
Pinch factor	H_{pinch}		1.3
Proton filling	H_{filling}		0.79
Luminosity	$\mathcal{L}_{ep}$	$\times 10^{32}\ cm^{-2}\,s^{-1}$	1.08

The luminosity $\mathcal{L}_{ep}$ is independent of the electron bunch charge and the collision frequency as long as their product, expressed in terms of the beam power $\mathcal{P}_e$, is constant. One can therefore write [20][40]

$$\mathcal{L}_{ep} = 4.8 \times 10^{30}\,\mathrm{cm}^{-2}\,\mathrm{s}^{-1} \cdot \frac{N_p}{10^{11}} \frac{10^{-6}\,\mathrm{m}}{\varepsilon_p^n} \frac{\gamma_p}{1066} \frac{10\,\mathrm{cm}}{\beta_p^*} \frac{\mathcal{P}_e}{22.6\,\mathrm{MW}} \frac{250\,\mathrm{GeV}}{\mathrm{E}_e} \cdot \mathcal{H} \tag{17}$$

The electron beam current $I_e = \mathrm{e}N_e f_{b,e} = 15$ mA, where $f_{b,e}$ is the inverse of the bunch interval (see Table 3). The electron beam power $\mathcal{P}_e = \mathrm{E}_e I_e d = 25.5$ MW, where d is the linac duty cycle. The proton beam current $I_p = 320$ mA and the energy stored per proton beam is 4.2 GJ. To calculate $H_{\mathrm{hourglass}}$, we set $\beta_e^* \approx \beta_p^*$ [36]. The value of H_{pinch} was taken from [25].

5 Acknowledgements

I would like to thank K. Oide and D. Zhou for helping me estimate some relevant beam properties at the SLC-type facility described in this note, and am grateful to K. Yokoya for valuable comments and suggestions.

References

[1] The LEP Collaborations, R. Barate et al., Phys. Lett. B **565**, 61 (2003).

[2] G. Aad et al. (Atlas Collab.), Phys. Lett. B **716**, 1 (2012).

[3] S. Chatrchyan et al. (CMS Collab.), Phys. Lett. B **716**, 30 (2012).

[4] J. Erler et al., Phys. Lett. B **486**, 125 (2000).

[5] M. McCullough, arXiv:1312.3322v6 (2014).

[6] A. Blondel and F. Zimmermann, arXiv:1112.2518v2 (2012).

[7] M. Koratzinos, arXiv:1511.01021v1 (2015).

[8] G. Moortgat-Pick et al., Eur. Phys. J. C **75**: 371 (2015).

[9] D. Asner et al., arXiv:1310.0763v3 (2013).

[10] J. L. Abelleira Fernandez, J. Phys. G: Nucl. Part. Phys. **39**, 075001 (2012).

[11] R. Belusevic, J. Mod. Phys. **8**, pp 1–16 (2017).

[12] B. Barish and J. Brau, Int. J. Mod. Phys. A **28**, 1330039 (2013).

[13] F. Zimmermann, private communication.

[14] I. Ginzburg et al., NIM **205**, 47 (1983); NIM **219**, 5 (1984).

[15] E. Saldin, E. Schneidmiller and M. Yurkov, Nucl. Instrum. Meth. A **472**, 94 (2001).

[16] C. Adolphsen et al., *The International Linear Collider Technical Design Report*, Volume 3.II; arXiv:1306.6328.

[17] G. Weber et al., Proc. 2nd ICFA Workshop on Possibilities and Limitations of Accelerators and Detectors, Les Diablerets, Switzerland, 4–10 Oct. 1979, pp 199–221.

[18] S. I. Alekhin et al., IHEP Preprint 87–48, Serpukhov (1987).

[19] A. N. Akay, H. Karadeniz and S. Sultansoy, Int. J. Mod. Phys. A **25**, No. 4, pp 4589–4602 (2010).

[20] M. Tigner, B. Wiik and F. Willeke, Proc. 1991 IEEE Part. Accel. Conf., San Francisco, California (1991).

[21] F. Zimmermann et al., Proc. EPAC2008, Genoa, Italy, pp 2847–2849 (2008).

[22] M. Benedikt, D. Schulte and F. Zimmermann, Phys. Rev. Spec. Topics — Accel. Beams **18**, 101002 (2015).

[23] F. Zimmermann, Nucl. Instrum. Meth. B **355**, pp 4–10 (2015).

[24] M. A. Furman, Proc. 1991 IEEE Particle Accelerator Conference, San Francisco, California, pp 422–424 (1991).

[25] O. Bruning et al., CERN-ACC-2017-0019 (2017).

[26] Y. Hao and V. Ptitsyn, Phys. Rev. Spec. Topics — Accel. Beams **13**, 071003 (2010).

[27] K. Schindl, *Space charge*, Proc. Joint US-CERN-Japan-Russia School on Particle Accelerators, Beam Measurements, Montreux, May 1998, edited by S. Kurokawa, S.Y. Lee, E. Perevedentsev, S. Turner, World Scientific, pp 127151 (1999).

[28] M. Benedikt and R. Garoby, CERN-AB-2005-009.

[29] A. Piwinski, in *Proc.* 9^{th} *Int. Conf. on High Energy Accelerators, Stanford* (1975).

[30] G. Parzen, Nucl. Instr. Meth. **A 256**, 231–240 (1987).

[31] F. Ruggiero and F. Zimmermann, Phys. Rev. Spec. Topics — Accel. Beams **5**, 061001 (2002).

[32] R. Brinkmann, Turk. J. Phys. **22**, pp 661-666 (1998).

[33] Ö. Yavas, Turk. J. Phys. **22**, pp 667-673 (1998).

[34] K. Wille, *The Physics of Particle Accelerators*, Oxford Univ. Press, 2000.

[35] F. Zimmermann, *Accelerator Physics and Technologis for Linear Colliders*, Physics 575 lecture notes, University of Chicago (2002).

[36] E. Cruz-Alaniz et al., Phys. Rev. Spec. Topics — Accel. Beams **18**, 111001 (2015).

[37] H. Damerau, Ph.D. Thesis, Technical Univ. Darmstadt, 2005.

[38] ALOHEP, https://alohep.hepforge.org; hosted by HepForge, IPPP Durham University.

[39] Y. C. Acar et al., arXiv:1608.02190 (2016).

[40] The THERA Book, edited by U. Katz, M. Klein, A. Levy and S. Schlenstedt, DESY 01-123F, Vol. 4, DESY-LC-REV-2001-062 (2001).